Emergent complexity in slowly driven stochastic processes

Antonio Carlos Costa* and Massimo Vergassola
Laboratoire de Physique de l'Ecole normale supérieure, ENS, Université PSL, CNRS, Sorbonne Université, Université de Paris, F-75005 Paris, France
(Dated: January 3, 2023)

We consider the distribution of first passage time events in the presence of non-ergodic modes that drive otherwise ergodic dynamics on a potential landscape. We find that in the limit of slow and large enough fluctuations the distribution of first passage time events, $f(t)$, exhibits heavy tails dominated by a power law with exponent $f(t) \sim t^{-2}$, and corrections that depend on the strength and the nature of fluctuations. We support our theoretical findings through direct numerical simulations in illustrative examples.

I. INTRODUCTION

Complex dynamics are ubiquitous in the natural world. Despite their intrinsic irregularity and unpredictability, they can nonetheless exhibit coherent and universal emergent properties Of particular importance in the study of complex systems is the understanding of the time taken for rare events to occur [1–3]. Notable examples include natural disasters [4] or the spreading of a virus [5]. In fact, first passage times are central to many fields within physics and beyond, with important examples stemming from chemistry, biology and finance (see, e.g., [6–12] and references therein). Biology in particular is ripe with examples where time is of the essence [13], such as fertilization [14], intracellular events [15–21], search processes (e.g., foraging or chemotaxis) [22–24], neural activity [25, 26] or population dynamics [27].

We here consider the estimation of first passage time distributions (FPTDs) from finite-time observations in an experimental context. In particular, we are interested in systems with intrinsic time scales comparable to the observation time, for which weak ergodicity breaking becomes evident [28, 29]. Such dynamics can be found for instance in glassy systems [30–33], where the time scales of equilibration are so long that one can decompose the dynamics into a stationary component and an "aging" component that breaks time-translation invariance.

Our main inspiration comes from the less traditional branch of the physics of animal behavior [34, 35]. Remarkably, recent advances in machine vision (see, e.g., [36–39]) have resulted in an explosion of high spatio-temporal resolution behavioral data. Analysis of fine-scale posture movements shows that, much like the run-and-tumble behavior of bacteria [40], more complex organisms also exhibit stereotyped behaviors, albeit with a more intricate structure [41–48]. The notion of stereotypy in behavior inherently stems from the time scale separation between variations on what is defined as a behavioral state, and the transitions between behavioral states, much like a particle hopping between wells in a potential landscape. For example, while foraging for food the nematode worm *C. elegans* transitions between coarse-grained "runs" and "pirouettes", which are stereotyped sequences of finer scale movements [48, 49]. However, unlike the particle hopping among potential wells which has a characteristic exponential distribution of transition rates, the time spent in a given behavior can be heavy-tailed (see, e.g. Fig. 4E of [48] or Fig. 3 of [50]). We here hypothesize that such heavy-tailed distributions reflect the slow continuous modulation of behavior on longer time scales, resulting from environmental factors or fluctuating internal states driven by neuromodulation, such as hunger, stress or arousal (see, e.g., [51–53]). Indeed, it has been shown that *C. elegans* continuously modulates its rate of reorientation events to explore larger and larger arenas in search for food [54]. In order to truly capture the multiscale nature of behavior, we therefore need to account for the fact that it can be modulated on time scales comparable to the observation time.

We introduce a general model of behavior in which the pose dynamics evolves in potential landscapes that fluctuate over time. We then study how these dynamics impact the estimation of the distribution of times spent in a given behavior. In section II we introduce our phenomenological description of the behavioral dynamics, decomposing it into ergodic dynamics on a potential landscape and the non-ergodic modulation of the landscape. We then derive a general result for the distribution of first passage times in section III, which we illustrate through direct numerical simulations of three example systems in section IV.

II. SLOWLY DRIVEN ERGODIC DYNAMICS

Given a set of observations of animal locomotion (e.g. from video imaging), we consider that the dynamics can be decomposed into ergodic and non-ergodic components. The former are the state-space variables that mix sufficiently well and define the potential wells that correspond to the stereotyped behaviors ; the latter non-ergodic components evolve on time scales comparable to the observation time and slowly modulate the potential landscape. The full dynamics is thus given by

* antonio.costa@phys.ens.fr

$$\begin{cases} \dot{\vec{X}} = F(\vec{X}, \vec{\lambda}) \\ \tau_\lambda \dot{\vec{\lambda}} = G(\vec{X}, \vec{\lambda}) \end{cases} , \tag{1}$$

where $\vec{X} \in \mathbb{R}^D$ represents the ergodic components, $\vec{\lambda} \in \mathbb{R}^{D_\lambda}$ represents the non-ergodic degrees of freedoms, F and G are nonlinear, possibly noisy, functions, and τ_λ is assumed to be of the order of the measurement time T_{exp}, $\tau_\lambda = \mathcal{O}(T_{\text{exp}})$, such that the $\vec{\lambda}$ dynamics do not mix. Given the time scale separation between the dynamics of $\vec{X}$ and $\vec{\lambda}$, we assume that the dynamics of $\vec{X}$ is well approximated by quasi-stationary Fokker-Planck dynamics $\dot{\rho} = \mathcal{L}\rho$, where $\mathcal{L}$ represents the Fokker-Planck operator. Since we are primarily interested in the long time scale behavior of the system, we consider a projection of the dynamics onto the slowest mode of $\mathcal{L}$, yielding a generalized Langevin equation [55, 56] with history-dependent friction and fluctuations. Assuming that we can sample the system on a time scale longer than the noise correlation time, we obtain an effective overdamped description :

$$\dot{\vec{X}} = F(\vec{X}, \vec{\lambda}) \Rightarrow \dot{x} = -\partial_x U(x, \lambda) + \sqrt{2T_x}\eta_x(t) , \tag{2}$$

where T_x captures the effective temperature, η_x is Gaussian white noise, and λ is a slow control parameter that modulates the effective potential landscape on slow time scales. Similarly, we consider that λ also obeys an effective overdamped Langevin equation,

$$\dot{\lambda} = -\tau_\lambda^{-1}\partial_\lambda V(\lambda) + \sqrt{2T_\lambda \tau_\lambda^{-1}}\eta_\lambda(t), \tag{3}$$

where V is assumed to be uncoupled from the dynamics of x for simplicity, T_λ captures the degree of fluctuations in λ and η_λ is Gaussian white noise.

III. FIRST PASSAGE TIME DISTRIBUTIONS

We are primarily interested in studying the time spent in a given behavioral state. Within the context of the Langevin dynamics of Eq. 2, this is given by the first passage time to reach an energy barrier x_f from the bottom of the potential x_0, defined as,

$$\tau_{x_0,x_f}(\lambda) = \inf\{\tau : x(t+\tau, \lambda) = x_f | x(t, \lambda) = x_0\} . \tag{4}$$

Despite the general interest in this concept, finding analytical expressions for the density of first passage time events is generally a formidable task [57]. Remarkably few closed-form expressions for the FPTD are known, with most results concerning only the mean first passage time (MFPT) which is more tractable (see, e.g., [1, 6, 9]). However, the MFPT provides only limited information on the first passage events, especially when multiple time scales are involved [15]. Here, we are interested in studying the behavior of the full first passage time distribution, with particular focus on its long time behavior in the presence of weakly non-ergodic dynamics for the general dynamics of Eqs. 2 and 3.

As previously discussed, the measurement time T_{exp} essentially separates ergodic from non-ergodic dynamics. In addition, it also sets a lower bound on the slowest observed hopping rates $\omega_{\min} \sim T_{\text{exp}}^{-1}$, such that when $\tau_\lambda = \mathcal{O}(T_{\text{exp}})$ we can make an adiabatic approximation and assume that transition events occur within a nearly static potential. For a given hopping rate ω, the FPTD is given by

$$f(t, \omega) = \omega e^{-\omega t} ,$$

where $\omega(\lambda) = 1/\tau_{x_0,x_f}(\lambda)$ is the dominating slow kinetic transition rate which implicitly depends on the dynamics of λ. Over multiple realizations of a finite-time experiment, we expect that when $\tau_\lambda \sim T_{\text{exp}}$ the distribution of first passage times, $f(t)$, will be given by the expectation value of $f(t, \omega)$ over the distribution of ω, $p(\omega)$, weighted by the effective number of transition observed within T_{exp}, which is proportional to ω. Marginalizing over ω we get,

$$f(t) \sim \int_{\omega_{\min}}^{\omega_{\max}} p(\omega)\omega^2 e^{-\omega t} d\omega. \tag{5}$$

While the barrier height is going to depend on the dynamics of a slow control parameter λ, the tail of the distribution is going to be dominated by instances in which the barrier height is the largest, motivating the use of Kramers approximation (see, e.g., [2]),

$$\omega(\lambda) = \omega_0 \exp\left\{-\frac{\Delta U(\lambda)}{T_x}\right\}, \tag{6}$$

where $\Delta U(\lambda) = U(x_f, \lambda) - U(x_0, \lambda)$ and ω_0 is a constant. Given that λ obeys an overdamped Langevin equation, Eq. 3, the distribution of λ is given by the Boltzmann weight

$$p(\lambda) \sim \exp\left\{-\frac{V(\lambda)}{2T_\lambda}\right\}. \tag{7}$$

Leveraging Eqs. 5,6,7 we can obtain an asymptotic approximation of the FPTD in the large t limit (see Appendix A)

$$f(t) \sim t^{-2} \exp\left\{-\frac{V(\Delta U^{(-1)}(T_x \log(\omega_0 t)))}{2T_\lambda}\right\} , \tag{8}$$

where $\Delta U^{(-1)}(\cdot)$ represents the inverse function of the potential difference defined by Eq. 6 and we have kept

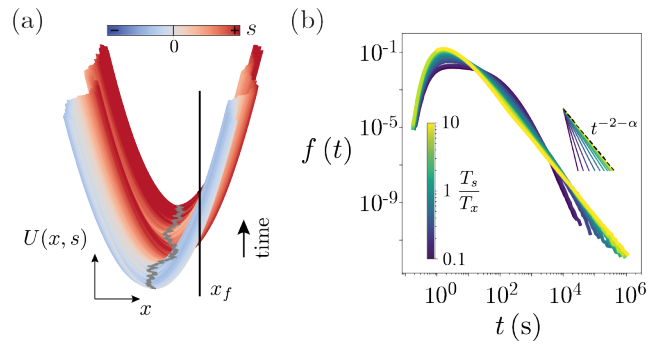

FIG. 1. Heavy-tailed first passage time distributions for a slowly-driven overdamped harmonic oscillator. (a) We simulate the dynamics of a particle in a harmonic oscillator while slowly driving the potential landscape, and estimate the distribution of times it takes to reach x_f. The gray line represents the minimum of potential, $x_0 = s$, and the color scheme different values of s. See Appendix C for simulation details. (b) FPTDs obtained from direct numerical simulations of Eq. 9 for different values of the temperature T_s that controls the level of fluctuations for the parameter driving the slow variations of the potential landscape. As predicted, the tail of the distribution behaves as a power law with an exponent $f(t) \sim t^{-2-\alpha}$, with $\alpha = \frac{T_x}{2T_s}$. The color scheme represents different ratios of temperatures, and the black dashed line the $T_s \to \infty$ limit.

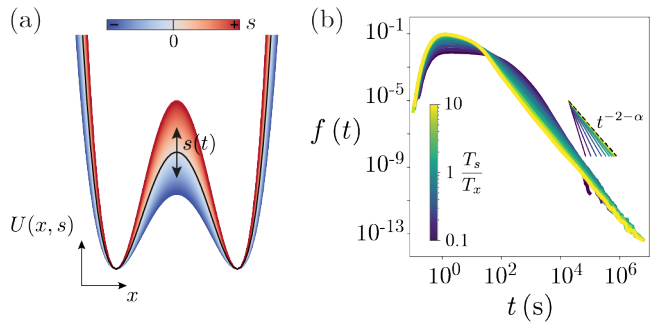

FIG. 2. Heavy-tailed first passage time distribution of a slowly-driven double-well potential. (a) Schematic of the variation in the double-well potential with s (colored from blue to red; the black line represents $s = \mu_s$). See Appendix C for simulation details. (b) FPTDs from direct numerical simulations of Eq. 11 for different values of T_s. As expected, the tail of the distribution behaves as a power law $f(t) \sim t^{-2-\alpha}$, where $\alpha = \frac{T_x}{4T_s}$ (colored line). The black dashed line represents the $T_s \to \infty$ limit.

only the dominant order of the approximation detailed in Appendix A. For very general conditions on $V(\lambda)$ and $U(x, \lambda)$, we thus get $f(t) \sim t^{-2}$ for $t \to \infty$ and $T_\lambda \gg 1$. In the following section we will demonstrate the validity of this result in three illustrative examples.

IV. ILLUSTRATIVE EXAMPLES

A. Slowly driven harmonic oscillator

Consider that x evolves in a harmonic potential, $U(x, s) = (x - sx_f)^2$, that is driven by a slow parameter s that fluctuates within $V(s) = s^2/2$, pushing $U(x, s)$ closer or further from x_f in a time scale τ_s, Fig. 1(a). The equations of motion are given by a set of Ito stochastic differential equation, corresponding to coupled Ornstein-Uhlenbeck processes,

$$\begin{cases} dx_t = -(x_t - s_t x_f)dt + \sqrt{2T_x}dW_t \\ ds_t = -\tau_s^{-1} s_t + \sqrt{2T_s\tau_s^{-1}}dW_t \end{cases} , \tag{9}$$

where T_x and T_s captures the degree of fluctuations, dW_t is a Wiener Gaussian white noise process. We are interested in the density of first passage time events from the minimum of the potential $x_0 = s$ to $x_f = 1$, for which it is challenging to find a closed form analytical expression, even when $s(t) = s \in \mathbb{R}$ [57]. In Appendix B, we derive the FPTD in Laplace space [58] and leverage it to estimate the FPTD through numerical inversion [59] for varying values of τ_s (as in Ref. [60]), see Fig. A2. We find that when s fluctuates fast enough, $\tau_s \to 0$, we can average out s and get the simpler dynamics $dx_t = -(x_t - \langle s \rangle x_f)\, dt + \sqrt{2T_x}dW_t$. In this case, the FPTD is well approximated by $f(t) \approx f(t, \langle \omega \rangle) = \langle \omega \rangle e^{-\langle \omega \rangle t}$, where $\langle \omega \rangle$ is the average hopping rate which is set by $\langle s \rangle$. Even when $\tau_s > 0$ but short, it is possible to obtain a self-consistent Markovian dynamics for $x(t)$ (see e.g., [1]). In this case, the distribution of first passage times is still dominantly exponential, but with a corrected first passage time which depends on the ratio of temperatures T_s/T_x and the slow time scale τ_s. However, as we have shown in the previous section and in Appendix A, when $\tau_s = \mathcal{O}(T_{\text{exp}})$, the distribution of first passage times becomes heavy-tailed. In this limit, we can leverage Eq. 8 to derive an asymptotic approximation to the distribution of first passage times. The tail of the distribution will be dominated by low ω values, which correspond to $|s| >> 1$. In this limit, the barrier height primarily behaves as $\Delta U(s) = s^2/2 + \mathcal{O}(s)$. In addition, since $V(s) = s^2/2$, we see that $V(\Delta U^{-1}(x)) = x$ and Eq. 8 yields (see Appendix A for details),

$$f(t) \sim t^{-2-\frac{T_x}{2T_s}} , \tag{10}$$

which matches what we obtain from direct numerical simulations of Eq. 9, see Figs. 1(b), A2 and A3(a).

B. Slowly-driven double-well potential

We now consider a symmetric double-well potential in which the barrier height is slowly modulated according to an Ornstein-Uhlenbeck process, Fig. 2(a),

$$\begin{cases} dx_t = -4s_t^2 x_t(x_t - 1)^2 dt + \sqrt{2T_x}dW_t \\ ds_t = -\tau_s^{-1}(s_t - \mu_s)dt + \sqrt{2T_s\tau_s^{-1}}dW_t \end{cases} , \tag{11}$$

where all the parameters are the same as in Eq. 9 with an extra μ_s that represents the expectation value of s, which we set as $\mu_s = 1$. In this case, we have a quartic potential for x, $U(x,s) = s^2(x^2-1)^2$, which yields $\Delta U(s) = s^2$. Since $V(s) = s^2/2$, we see that $V(\Delta U^{-1}(x)) = x/2$ and Eq. 8 yields (see Appendix A for details),

$$f(t) \sim t^{-2-\frac{T_x}{4T_s}} , \tag{12}$$

matching what we find through direct numerical simulations of Eq. 11, see Figs. 2(b) and A3(b).

C. Rugged parabolic potential

Finally, we consider a rugged parabolic potential as a simple model of the rough energy landscapes found across complex systems, from glasses to proteins (see, e.g., [19, 20, 61]). We construct a rugged landscape by superimposing a sinusoidal perturbation onto a harmonic potential [62], $U(x,s) = U_0(x,s) + U_1(x)$, where $U_0(x,s) = (x-s)^2/2$ and $U_1(x) = -\cos(2\pi k x)/(k\pi)$. The corresponding dynamics are given by,

$$\begin{cases} dx_t = -\left(x_t - s_t + 2\sin(2\pi k x_t)\right)dt + \sqrt{2T_x}dW_t \\ ds_t = -\tau_s^{-1}s_t + \sqrt{2T_s\tau_s^{-1}}dW_t \end{cases} , \tag{13}$$

where k sets the number of smaller barriers between the global minimum of the potential and $x_f = 1$. We set $k = 10$ resulting in a rugged potential as illustrated in Fig. 3(a). In this case, since $U(x,s)$ is not as simple as before, it is more challenging to derive the correction terms to the power law. However, it has been shown [62] that by spatial averaging of $U_1(x) = -\cos(2\pi k x)/(k\pi)$ over one period, the resulting hopping rate is simply corrected by a constant prefactor $\omega = I_0^{-2}(k^{-1}\pi^{-1}T_x^{-1})\omega_0$, where I_0 is the modified Bessel function and ω_0 is the hopping rate in the absence of the sinusoidal perturbation (from $U_0(x,s) = (x-s)^2/2$). As such, we expect the asymptotic behavior of $f(t)$ to be the same as for the slowly driven harmonic potential, Eq. 10. Indeed, this is what we observe in Figs. 3(b), A3(c).

V. DISCUSSION

Inspired by quantitative analysis of animal behavior, we here examined how the existence of slow non-ergodic modes impacts the statistics collected experimentally, focusing on the distribution of first passage time events. Our results show the emergence of heavy-tailed distributions. In particular, we find that the distribution asymptotes to a power law with an exponent $f(t) \sim t^{-2}$ in the limit of large fluctuations, regardless of the details of the dynamics. As remarked in the Introduction, our results have important implications to a wide variety of fields, and we here discuss some of these in detail.

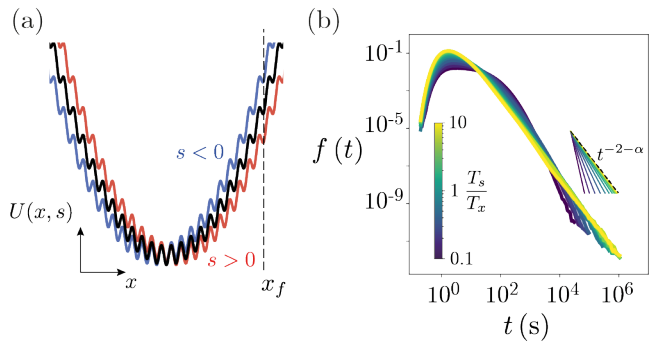

FIG. 3. Heavy-tailed first passage time distribution in slowly driven rugged parabolic potential. (a) We estimate the first passage time to reach x_f from the global minimum of a rugged parabolic potential. See Appendix C for simulation details. (b) FPTDs from direct numerical simulations of Eq. 13 for different values of T_s. As expected, the tail of the distribution behaves as a power law $f(t) \sim t^{-2-\alpha}$ (colored lines) with $\alpha = \frac{T_x}{2T_s}$. The black dashed line corresponds to the $T_s \to \infty$ limit.

In the context of animal behavior, heavy-tailed first passage times with an exponent $f(t) \approx t^{-2}$ have been found extensively across multiple species, from bacteria [63], termites [64] and rats [65] to marine animals [66, 67], humans [68] and even fossil records [69]. In the context of search behaviors (e.g., when foraging for food), such observations have led researchers to hypothesize that Lévy-flights (power law distributed run lengths) are efficient search strategies and thus evolutionarily favorable [70–74]. However, we here show that such fat tails may emerge when the animal is continuously adapting its behavior (slowly modulating the potential landscape), even in the absence of external drives. In fact, even in the absence of active control by the nervous system, morphological changes resulting from maturation and development may be enough to give rise to the emergent power law behavior, as was observed in fly larvae with a disrupted nervous system [75].

Importantly, power laws have been observed in a wide variety of systems, from solar flares [76, 77] to the brain [78] and different hypotheses have been put forward to explain their emergence (for a review see e.g. [79]). Among these, work inspired by phase transitions in statistical mechanics associates power laws to "criticality", mostly due to the fact that models inferred from the data appear to require fine-tuning of the model parameters to a special regime between two qualitatively different "phases" (see, e.g., [80]). However, as we have shown here, power laws can emerge without fine tuning and far from "criticality". Indeed, slow modes that evolve on time scales comparable to the observation time are challenging to infer from data, and can give rise to best-fit models that appear "critical". While some of the arguments we have put forward have also been proposed in other contexts [22, 81–83], we here place them into the framework of out-of-equilibrium statistical mechanics, explicitly connect-

ing the long time scale emergent behavior with the underlying effective fluctuations. In addition, unlike other approaches [82, 84], our framework does not require explicit external drives, but simply collective modes that evolve in a weakly non-ergodic fashion.

Our starting point is an effective description of the long time scale dynamics, and further work will be required to fully bridge between microscopic collective dynamics, and the emergent long time behavior of the first passage time distribution that we uncovered. For example, Fig. A2 shows that for intermediate values of $1 \ll \tau_\lambda \ll T_{\rm exp}$ the FPTD behaves as a truncated power law with an effective exponent that is slightly smaller that -2, which goes beyond arguments presented here. What are the minimum τ_λ and T_λ for power laws to be measurable, and how do simple exponentials ($\tau_\lambda \ll T_{\rm exp}$) transition to power law behavior? These are important questions if one hopes to test our predictions in an experimental context (using for example a set-up akin to the ones used to test stochastic resonance [85, 86]). Additionally, we note that when $\tau_\lambda \gg T_{\rm exp}$, the distribution of initial conditions is important to define the emergent behavior, Fig. A4. Inspired by experiments in animal behavior, which are typically done with multiple animals, we here assume that the initial condition for the slow mode is sampled according to its Boltzmann distribution $\lambda(t=0) \sim e^{-\frac{V(\lambda)}{2T_\lambda}}$, reflecting the variability across individuals. In this case, the emergent behavior we have derived holds true from $\tau_\lambda \sim T_{\rm exp}$ to $\tau_\lambda \to \infty$. However, if the variability across experiments is smaller than that of the Boltzmann distribution, the $\tau_\lambda \to \infty$ limit will differ from the behavior at $\tau_\lambda \sim T_{\rm exp}$. Indeed, in the limit $\tau_\lambda \to \infty$ the observed distribution of λ is directly set by the initial condition. As such, if the variance of the initial distribution of λ is smaller than that of the Boltzmann distribution, the temperature T_λ in our derivation should be changed to a new effective temperature $T_\lambda^0 < T_\lambda$ reflecting the lower variance of the initial conditions. Making this transformation we still get a power law distribution of first passage times, but with a modified exponent that reflects the lower variance. Naturally, for $\tau_\lambda \sim T_{\rm exp}$ our result is independent of the initial conditions, since λ will be distributed according to the Boltzmann distribution.

To conclude, we have considered the effect of slow non-ergodic modulations and theoretically captured their effects on the distribution of first passage times, a result that we believe is widely relevant to a range of natural systems.

ACKNOWLEDGEMENTS

We thank Adrian van Kan, Stéphan Fauve, Federica Ferretti, Tosif Ahamed and Arghyadip Mukherjee for comments and lively discussions. This work was supported by the LabEx ENS-ICFP: ANR-10-LABX-0010/ANR-10-IDEX-0001-02 PSL*. AC also acknowledges useful discussions at the Aspen Center for Physics, which is supported by National Science Foundation Grant PHY-1607611.

Appendix A: General derivation

We here derive the expression for the first passage time distribution in a fluctuating potential landscape. Since $\omega = \omega_0 \exp\{-\Delta U(\lambda)/T_x\}$, we have $\lambda(\omega) = \Delta U^{(-1)}(-T_x \log(\omega/\omega_0))$, where ω_0 is a typical (fast) frequency of the hopping dynamics. The distribution $p(\omega)$ obeys $p(\omega)d\omega = p(\lambda)d\lambda$, and it is thus given by

$$p(\omega) \sim \exp\left\{-\frac{V(\lambda(\omega))}{2T_\lambda}\right\} \frac{T_x/\omega}{\partial_\lambda \Delta U(\lambda)}\,.$$

By using the adiabatic limit, Eq. 5, we get

$$f(t) \propto \int_{\omega_{\min}}^{\omega_{\max}} \exp\left\{-\frac{V(\lambda(\omega))}{2T_\lambda}\right\} \frac{T_x}{\partial_\lambda \Delta U(\lambda)} \omega e^{-\omega t} d\omega. \tag{A1}$$

The exponential factor $e^{-\omega t}$ restricts the contributions to $\omega \sim 1/t$, which motivates the change of variable $\omega = \frac{\theta}{t}$. The above integral is then recast in the form

$$f(t) \propto t^{-2} \int_{\theta_{\min}(t)}^{\theta_{\max}(t)} \frac{\exp\left\{-\theta - \frac{V(\lambda(\theta))}{2T_\lambda} + \log(\theta)\right\}}{\partial_\lambda \Delta U(\lambda(\theta))} d\theta, \tag{A2}$$

where $\lambda(\theta) = \Delta U^{(-1)}\left(-T_x \log\left(\frac{\theta}{\omega_0 t}\right)\right)$, $\theta_{\min}(t) = \omega_{\min} t$ and $\theta_{\max}(t) = \omega_{\max} t$.

To grasp the structure of the integral, it is convenient to consider first the special case where V and ΔU can be written as a power series expansion $V(\lambda) \sim a\lambda^n$ and $\Delta U(\lambda) \sim b\lambda^n$, $a, b \in \mathbb{R}$ with an equal dominant (at large values of the argument, see below) exponent n. The integral reduces then to the form

$$f(t) \propto t^{-2-\frac{aT_x}{2bT_\lambda}} \int_{\theta_{\min}}^{\theta_{\max}} \frac{\theta^{1+\frac{aT_x}{2bT_\lambda}} e^{-\theta}}{\left(-\log\left(\frac{\theta}{\omega_o t}\right)\right)^{1-\frac{1}{n}}} d\theta\,.$$

The power law factor in t yields the scaling result announced in the main text. It remains to verify that the time dependencies at the denominator of the integrand and the limits of integration do not spoil the behavior at large times. This is verified by noting that the numerator of the integrand has the structure of an Euler-Γ function of order $2 + \frac{aT_x}{2bT_\lambda}$. The integrand has its maximum at $\theta^* = 1 + \frac{aT_x}{2bT_\lambda}$, decays over a range of values of order unity and vanishes at the origin. In that range, the argument of the power at the denominator $\log(\omega_0 t) - \log(\theta) \simeq \log(\omega_0 t)$, which yields the final scaling with subdominant logarithmic corrections

$$f(t) \sim t^{-2-\frac{aT_x}{2bT_\lambda}} \times \log(\omega_0 t)^{\frac{1}{n}-1}. \tag{A3}$$

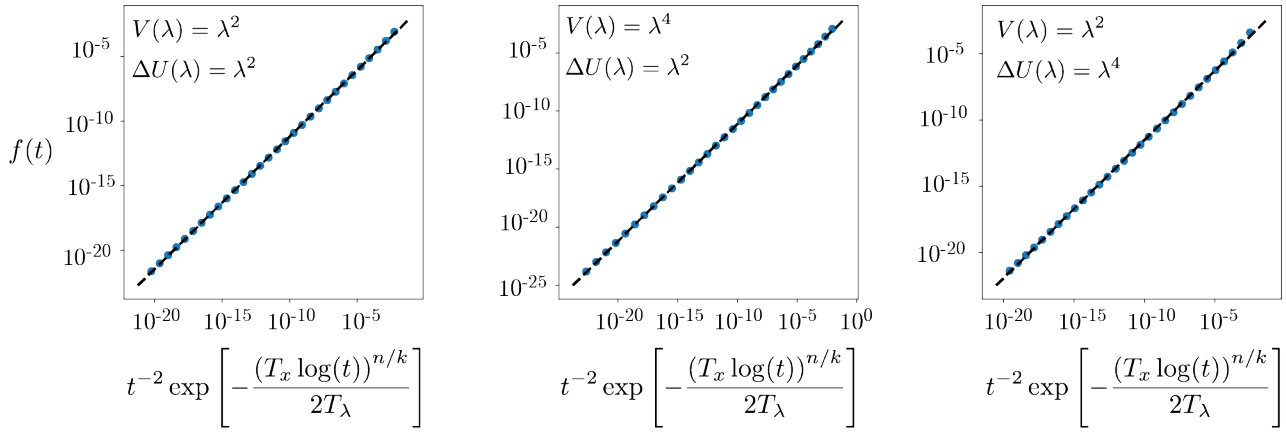

FIG. A1. Numerical integration of $f(t)$ for different choices of $V(\lambda)$ and $\Delta U(\lambda)$, compared to the asymptotic approximation of Eq. A5 (black dashed line) with $T_x = 0.1$ and $T_\lambda = 0.2$.

To complete the argument, we note that the time dependency of $\theta_{\min}$ is not an issue as long as values $\theta \sim O(1)$ are in the integration range. In practice, this means that the minimum hopping rate $\omega_{\min}$ should be comparable to (or larger than) the measurement time, $\omega_{\min}^{-1} \sim \mathcal{O}(T_{\exp})$.

Before moving to the general case, two remarks are in order. First, for $\omega_0 t \gg 1$ the functions V and $\partial_\lambda \Delta U$ that appear in Eq. A2 have their argument $\lambda \gg 1$. The dominant behavior of the two functions should then be understood for large values of their arguments. Second, the denominator $\partial_\lambda \Delta U$ could *a priori* be included in the exponential at the numerator but this does not modify our conclusion. It is indeed easy to verify that the maximum θ^* and the decay range would not be not shifted at the dominant order (and this holds also for the general case considered hereafter).

We can now consider the general case with different dominant exponents $V(\lambda) \sim a\lambda^n$ and $\Delta U(\lambda) \sim b\lambda^k$, $a, b \in \mathbb{R}$. The argument of the exponential in Eq. A2

$$\mathcal{L}(\theta) = -\theta - \frac{V(\lambda(\theta))}{2T_\lambda} + \log(\theta) \ , \tag{A4}$$

has its maximum at θ^*, defined by the implicit equation

$$\theta^* = 1 + \frac{T_x}{2T_\lambda}\frac{\partial_\lambda V(\lambda(\theta^*))}{\partial_\lambda \Delta U(\lambda(\theta^*))} = 1 + \frac{T_x}{2T_\lambda}\frac{an}{bk}\lambda^{n-k} \ ,$$

where we have used

$$\partial_\theta V(\lambda) = \partial_\lambda V(\lambda) \times \frac{d\lambda(\theta)}{d\theta} \ ; \quad \frac{d\lambda(\theta)}{d\theta} = -\frac{T_x/\theta}{\partial_\lambda \Delta U(\lambda)} \ .$$

For $n < k$, the maximum $\theta^* \simeq 1$ and the integrand decays in a range of order unity. Indeed, it is checked that the dominant order of the derivatives $\partial^p \mathcal{L}$ $(p \geq 2)$ at $\theta = \theta^*$ coincide with those of $\log(\theta)$. It follows that $\mathcal{L}(\theta) - \mathcal{L}(\theta^*) \simeq \log(\theta/\theta^*) - (\theta - \theta^*)$. The resulting integral over θ is an Euler Γ-function of order two, which indeed forms at values $O(1)$. In that range, $\lambda \sim \left(\frac{T_x}{b}\log(\omega_0 t)\right)^{1/k}$ and the integral is then approximated by $\exp\{\mathcal{L}(\theta^*)\}$ and the function $f(t)$ in Eq. A2 by

$$f(t) \sim t^{-2}\exp\left\{-\frac{a\left(\frac{T_x}{b}\log(\omega_0 t)\right)^{n/k}}{2T_\lambda}\right\} \ .$$

The factor at the denominator in Eq. A2 is $O\left[\exp\left\{(1/k-1)\log[\log(\omega_0 t)]\right\}\right]$ and thus of the same order as terms that we have discarded in our approximation so we neglect it as well. Since the integral over θ forms for values $O(1)$, the constraint on the minimum hopping rate is the same as for the $n = k$ case, i.e., $\omega_{\min}^{-1} \sim \mathcal{O}(T_{\exp})$.

For $n > k$, the maximum $\theta^* \sim (\log \omega_0 t)^{n/k-1}$, which is now large. The dominant order of the derivatives $\partial^p \mathcal{L}$ $(p \geq 2)$ at $\theta = \theta^*$ is given by $(-1)^{p-1}(p-1)!\,(\theta^*)^{-p-1}$, that is they coincide with those of $\theta^* \log(\theta)$. It follows that $\mathcal{L}(\theta) - \mathcal{L}(\theta^*) \simeq \theta^*\left[\log(\theta/\theta^*) - (\theta - \theta^*)/\theta^*\right]$. The resulting integral over θ is an Euler Γ-function of (large) argument $\theta^* + 1$: its value is approximated by Stirling formula, which yields $\int (\theta/\theta^*)^{\theta^*} e^{-(\theta-\theta^*)}\, d\theta \simeq \sqrt{\theta^*}$. The $\sqrt{\theta^*}$ reflects the fact that the integral forms around the maximum at θ^* of the integrand over a range $\sqrt{\theta^*}$, which implies that the approximation $-\log(\theta/\omega_0 t) \simeq \log(\omega_o t)$ still holds, as in the previous cases $n \leq k$. The $\sqrt{\theta^*}$, as well as the $\log(\omega_0 t)^{1/k-1}$ coming from the denominator in Eq. A2, is subdominant with respect to terms that we have neglected in the expansion of $\mathcal{L}$. We therefore discard them from our final approximation for $n > k$:

$$f(t) \sim t^{-2}\exp\left\{-\frac{a\left(\frac{T_x}{b}\log(\omega_0 t)\right)^{n/k}}{2T_\lambda}\right\} \ .$$

Since the integral over θ forms for values $O\left((\log \omega_0 t)^{n/k-1}\right) \gg 1$, the condition $\omega_{\min}^{-1} \sim \mathcal{O}(T_{\exp})$ ensures *a fortiori* that the finite value of $\omega_{\min}$ does not affect the above result.

Discarding subdominant terms, in all three cases we

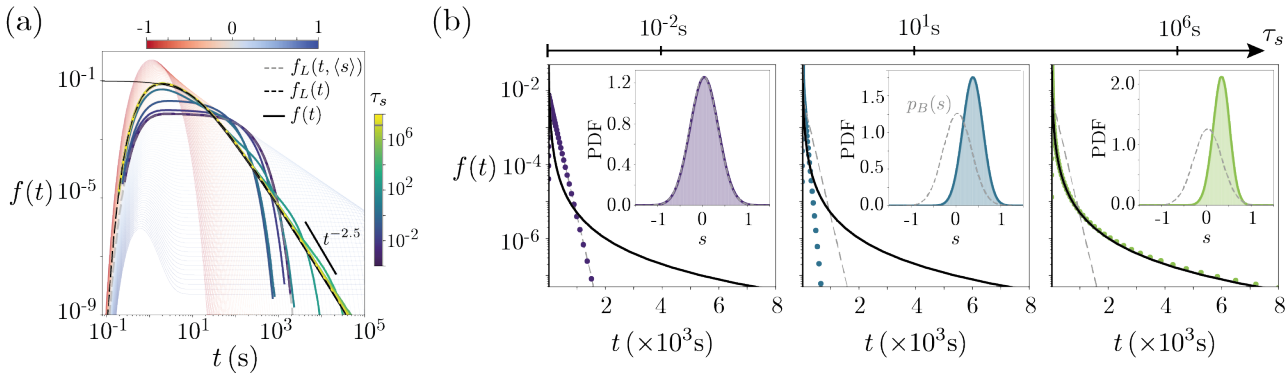

FIG. A2. Emergence of heavy-tails when the driving is sufficiently slow (a) First passage time distribution for different values of τ_s (colored from purple to yellow) show the emergence of heavy tails as $\tau_s \to \infty$. We also plot the full FPTDs $f_L(t,s)$, Eq. (A4), for different fixed values of s (color coded from red to blue). From these estimates, we highlight $f_L(t,\langle s\rangle = 0)$ (gray dashed line), which corresponds to the mean first passage time in the limit $\tau_s \to 0$ (purple line). We also plot $f_{\rm L}(t)$ (black dashed line), which corresponds to the adiabatic approximation of the FPTD obtained through a weighted average of the FPTDs obtained for fixed s, Eq. (A5); and $f(t)$, which corresponds to Eq. (10). (b) First passage times for 3 qualitatively different regimes and the corresponding distribution of s at the first passage event (inset). When $\tau_s \to 0$ (left) the distribution of s at the first passage time events corresponds to the Boltzmann distribution of s, $p(s) \sim e^{-V(s)/T_s}$ (gray dashed line in the inset), and the distribution of first passage times $f(t)$ matches the one obtained from a fixed $s = \langle s\rangle = 0$ (dashed line); when τ_s matches the time scale of x (middle), we observe that the mean first passage time is reduced, boosted by events in which the harmonic potential moves closer to the boundary as shown in the inset; finally, when $\tau_s \gg 1$, we observe the emergence of a heavy tailed first passage time accurately predicted by Eq. (10) (black line).

thus get the general expression,

$$f(t) \sim t^{-2} \exp\left\{ -\frac{a\left(\frac{T_x}{b}\log(\omega_0 t)\right)^{n/k}}{2T_\lambda} \right\}. \tag{A5}$$

To verify the validity of the above arguments, we show in Fig.A1 how, to dominant order, asymptotic predictions agree with a detailed numerical integration of Eq. A1 for $\Delta U(\lambda) = \lambda^k$ and $V(\lambda) = \lambda^n$.

Appendix B: First-passage time through an absorbing boundary in a harmonic oscillator

We here derive the first passage distribution for the harmonic oscillator of Eq. 9 but for fixed s, so for

$$dx_t = -(x_t - s x_f)dt + \sqrt{2T_x}dW_t, \tag{A1}$$

where $s \in \mathbb{R}$. The corresponding Fokker-Planck equation is given by

$$\begin{aligned}\partial_t \rho =& \mathcal{L}\rho\,;\\ \mathcal{L} =& \partial_x((x - s x_f)\bullet) + T_x \partial_x^2(\bullet)\,.\end{aligned}$$

We are interested in the distribution of first passage times from x_0 to the energy barrier located at x_f, derived in the Supplementary Information of [87]. We here reformulate this derivation and tune it to our particular case. The survival probability can be written as

$$S(x_f, t|x_0) = \int_{-\infty}^{x_f} P_{x_f}(x,t|x_0)dx\,,$$

where $P_{x_f}(x,t|x_0)$ is the propagator from $t=0$ to t with the constraint that $x < x_f$. In other words, we have an absorbing boundary condition at x_f, $P(x_f,t|x_0) = 0$. From the survival probability, the first passage density can be obtained as

$$f_{x_f}(t|x_0) = -\partial_t S_{x_f}(t|x_0).$$

The backward Kolmogorov equation for the propagator $P_{x_f}(x,t|x_0)$ is $\partial_t P_{x_f}(x,t|x_0) = \mathcal{L}^\dagger_{x_0} P_{x_f}(x,t|x_0)$, where $\mathcal{L}^\dagger_{x_0}$ is the adjoint of the generator of the stochastic process, $\mathcal{L}^\dagger_{x_0} = -(x_0 - s x_f)\partial_{x_0}\bullet + T_x \partial^2_{x_0}\bullet$. Integrating the backward Kolmogorov equation and then taking the time derivative we get

$$\begin{aligned}\partial_t S_{x_f}(t|x_0) &= \mathcal{L}^\dagger_{x_0} S_{x_f}(t|x_0)\\ \partial_t f_{x_f}(t|x_0) &= \mathcal{L}^\dagger_{x_0} f_{x_f}(t|x_0),\end{aligned}$$

which vanishes for $x_0 > x_f$, $f_{x_f}(0|x_0) = 0$, $f_{x_f}(t|x_f) = \delta(t)$. To solve for f we take the Laplace transform, $Lf_{x_f}(t|x) = \hat{f}_{x_f}(p|x)$

$$\begin{aligned}\int_0^\infty e^{-pt}\partial_t f_{x_f}(t|x_0)dt =& \mathcal{L}^\dagger_{x_0}\hat{f}_{x_f}(p|x_0)\\ e^{-pt} f_{x_f}(t|x_0)|_0^\infty + p\int_0^\infty e^{-pt} f_{x_f}(t|x_0)dt =& \mathcal{L}^\dagger_{x_0}\hat{f}_{x_f}(p|x_0)\\ f_{x_t}(0|x_0) + p\hat{f}_{x_f}(p|x_0) =& \mathcal{L}^\dagger_{x_0}\hat{f}_{x_f}(p|x_0)\\ (\mathcal{L}^\dagger_{x_0} - p)\hat{f}_{x_f}(p|x_0) =& 0\end{aligned}$$

where we performed integration by parts and made use of the initial condition. The unique solution to the above

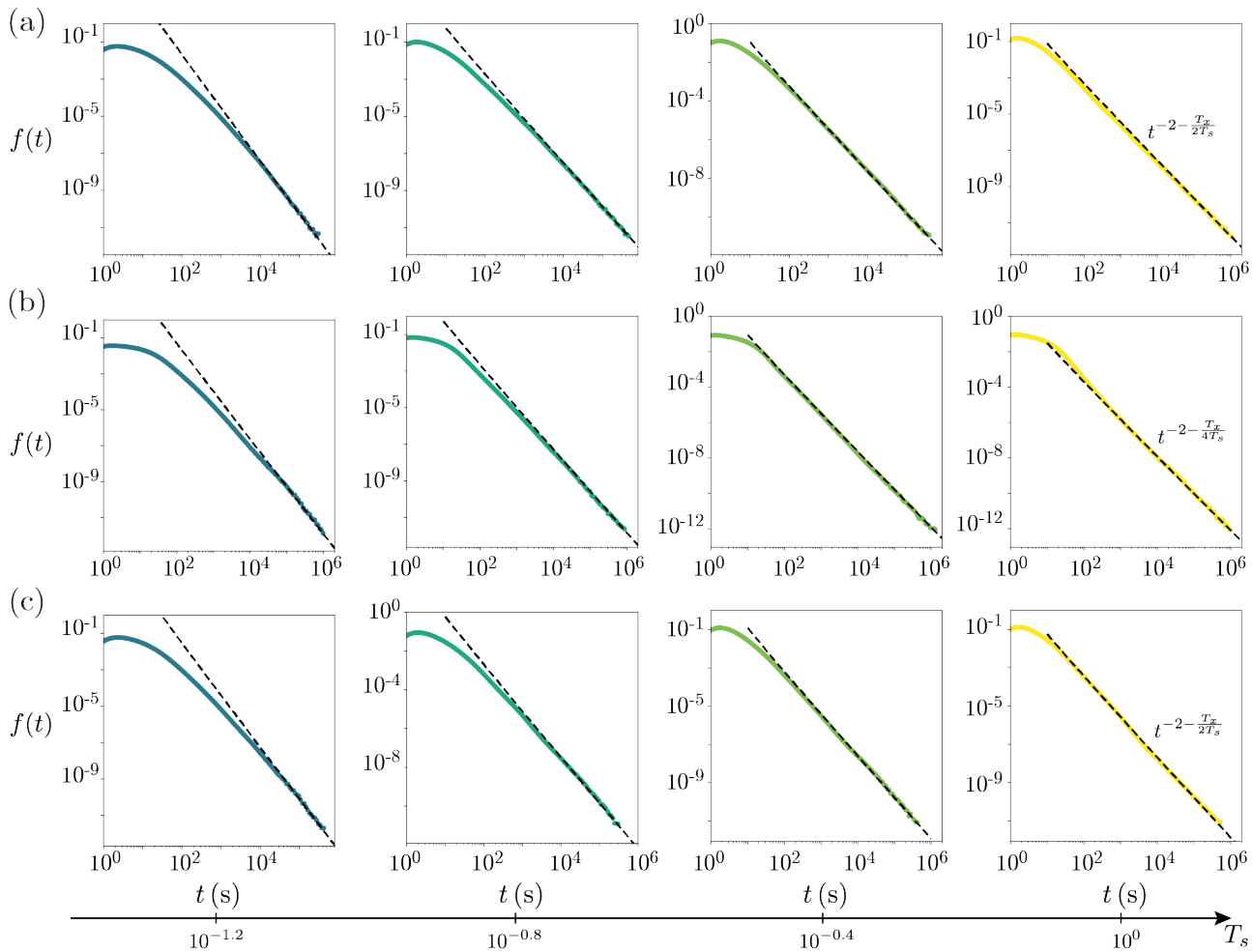

FIG. A3. Details of the accuracy of the asymptotic prediction for the behavior of the tail of $f(t)$ across temperatures T_s for the slowly driven harmonic oscillator (a), the slowly driven double well potential (b) and the slowly driven rugged parabolic potential (c).

problem is given by $\hat{f}_{x_f}(p|x_0) = v_p(x_0)/v_p(x_f)$, where $v_p(\bullet)$ is the unique increasing positive solution of the equation $(\mathcal{L}^\dagger_{x_0} - p)v_p = 0$ [58]. For the harmonic oscillator we get

$$-(x - sx_f)\partial_x v_p(x) + T_x \partial_x^2 v_p(x) - p v_p(x) = 0,$$

which we can solve by rewriting $v_p(x)$ as

$$v_p(x) = \exp\left\{\frac{x^2 - 2sx_f x}{4D}\right\} Z_p(x),$$

yielding,

$$T_x \partial_x^2 Z_p(x) + Z_p(x)\left[-p + \frac{1}{2} - \frac{(x - sx_f)^2}{4T_x}\right] = 0$$

Rescaling $x = \sqrt{T_x}y + sx_f$, and using the chain rule, $\partial_x^2 Z_p(x) = T_x^{-1}\partial_y^2 Z_p(y)$, we get,

$$\frac{d^2 Z_p(y)}{dy^2} + Z_p(y)\left(-\frac{y^2}{4} + \frac{1}{2} - p\right) = 0$$

which is Weber's parabolic cylinder differential equation, with solution,

$$Z_p(x) = D_{-p}\left[-\sqrt{T_x^{-1}(x - sx_f)^2}\right],$$

where D_α is the parabolic cylinder function. Thus,

$$v_p(x) = \exp\left\{\frac{x^2 - 2sx_f x}{4T_x}\right\} D_{-p}\left[-\sqrt{T_x^{-1}(x - sx_f)^2}\right] \tag{A2}$$

From this we can write an expression for the Laplace transform of the distribution of times for a particle to go from $x_0 = 0$ to $x_f = 1$,

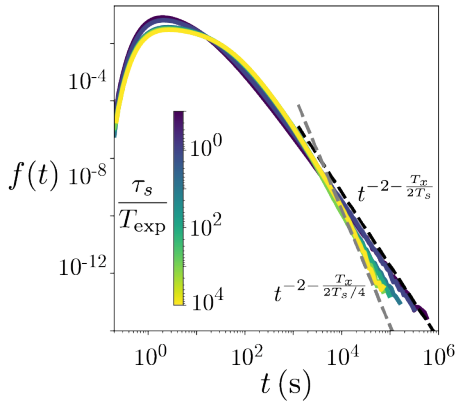

FIG. A4. First passage time distribution for different values of τ_s (colored from purple to yellow) when the initial condition is a narrower Boltzmann distribution with $T_s^0 = T_s/4$. As discussed in the main text, when $\tau_s \to \infty$ the FPTD exhibits a deeper power law exponent. When $\tau_s \sim T_{\rm exp}$ we recover the asymptotic behavior derived in Eq. 10.

$$\hat{f}_L(p,s) = \hat{f}_{x_f=1}(p|x_0=0) = \frac{v_p(x_0=0)}{v_p(x_f=1)} = e^{-\frac{1-2s}{4T_x}} \frac{D_{-p}\left[-\sqrt{s^2/T_x}\right]}{D_{-p}\left[-\sqrt{(1-s)^2/T_x}\right]}, \tag{A3}$$

which we can invert numerically to evaluate the first passage time distribution (see e.g. [88]),

$$f_L(t,s) = L^{(-1)}\left[\hat{f}_L(p,s)\right]. \tag{A4}$$

In Fig. A2(a) we used the method of de Hoog et al. [59] to numerically invert the Laplace transform and obtain the FPTDs for each fixed s. In addition, we estimate the adiabatic approximation of the full FPTD through,

$$f_L(t) = \int p(s) f_L(t,s) ds, \tag{A5}$$

where $p(s)$ is the distribution of the values of s during first passage time events.

Appendix C: Numerics

Simulations

Driven harmonic oscillator : We generate 1000 simulations of the dynamics of Eq. 9 through an Euler-scheme with a sampling time of $\Delta t = 10^{-4}$ s for $T_{\rm exp} = 10^7$ s and with initial condition $x(0) = 0$ and $s(0) \sim \mathcal{N}(0, \sqrt{T_s})$ is sampled according to the Boltzmann distribution. As for the parameter values, we take $T_x = 0.1$, $T_s = 0.1$ and vary τ_s in Figs. A2, A4, and fix $\tau_s = 10^3 \times T_{\rm exp}$ and vary T_s in Figs. 1, A3(a).

Driven double well potential: We generate 1000 simulations of the dynamics of Eq. 11 through an Euler-scheme with a sampling time of $\Delta t = 10^{-4}$ s for $T_{\rm exp} = 10^7$ s, $\tau_s = 10^3 \times T_{\rm exp}$ and with initial condition $x(0)$ which is randomly chosen as $x(0) = 1$ and $x(0) = -1$ with equal probability and $s(0) \sim \mathcal{N}(\mu_s, \sqrt{T_s})$ is sampled according to the Boltzmann distribution. As for the parameter values, we take $T_x = 0.15$ and vary T_s in Figs. 2, A3(b).

Driven parabolic potential: We generate 1000 simulations of the dynamics of Eq. 13 through an Euler-scheme with a sampling time of $\Delta t = 10^{-4}$ s for $T_{\rm exp} = 10^7$ s, $\tau_s = 10^3 \times T_{\rm exp}$ and with initial condition $x(0) = 0$ and $s(0) \sim \mathcal{N}(0, \sqrt{T_s})$ is sampled according to the Boltzmann distribution. As for the parameter values, we take $T_x = 0.1$ and vary T_s in Figs. 3, A3(c).

Numerical integration

We numerically integrate Eq. A1 with $\Delta U(\lambda) = \lambda^k$ and $V(\lambda) = \lambda^n$, through a Riemman sum using the midpoint rule from $\omega_{\rm min} = 5 \times 10^{-10}$ to $\omega_{\rm max} = 1$ with $\Delta\omega = 10^{-9}$, yielding the results of Fig. A1.

First passage time distribution estimation

From the simulations of $x(t)$, we first identify all segments, $[t_0, t_f]$, in which t_0 corresponds to the first time x returns to x_0 for the after reaching x_f, and t_f is the time first to reach x_f after t_0. We then build a normalized histogram of first passages times with logarithmic bins. We note that while for the slowly driven potential landscape the position of the minima of the potential are fixed at $x_0 = \pm 1$, for the slowly driven harmonic oscillator and the rugged parabolic potential the minima of the potential are driven by s. For practical reasons, in the numerical estimation of the FPTD we take $x_0 = \langle s \rangle = 0$, which has no practical impact due to the severe separation of time scales between the first passage time events and the relaxation to the well. In practice, even if $s \neq 0$, x is pushed from x to $x = s$ in a negligible time scale compared to the first passage time to x_f.

[1] P. Hänggi, *Escape over fluctuating barriers driven by colored noise,* Chemical Physics **180**, 157 (1994).

[2] N. G. Van Kampen, *Stochastic processes in physics and chemistry* (North-Holland, Amsterdam, 1981).

[3] S. Redner, *A Guide to First-Passage Processes* (Cambridge University Press, 2001).

[4] I. Wijesundera, M. N. Halgamuge, T. Nanayakkara, and T. Nirmalathas, *Natural Disasters, When Will They Reach Me?*, Springer Natural Hazards (Springer Singapore, Singapore, 2016).

[5] A. K. Verma, A. Bhatnagar, D. Mitra, and R. Pandit, *First-passage-time problem for tracers in turbulent flows applied to virus spreading,* Phys. Rev. Research **2**, 033239 (2020).

[6] A. Szabo, K. Schulten, and Z. Schulten, *First passage time approach to diffusion controlled reactions,* The Journal of Chemical Physics **72**, 4350 (1980).

[7] S. Condamin, V. Tejedor, R. Voituriez, O. Bénichou, and J. Klafter, *Probing microscopic origins of confined subdiffusion by first-passage observables,* Proceedings of the National Academy of Sciences **105** (2008), 10.1073/pnas.0712158105.

[8] O. Bénichou and R. Voituriez, *From first-passage times of random walks in confinement to geometry-controlled kinetics,* Physics Reports **539**, 225 (2014).

[9] O. Bénichou, T. Guérin, and R. Voituriez, *Mean first-passage times in confined media: from Markovian to non-Markovian processes,* Journal of Physics A: Mathematical and Theoretical **48**, 163001 (2015).

[10] K. R. Ghusinga, J. J. Dennehy, and A. Singh, *First-passage time approach to controlling noise in the timing of intracellular events,* Proceedings of the National Academy of Sciences **114** (2017), 10.1073/pnas.1609012114.

[11] R. Chicheportiche and J.-P. Bouchaud, Some applications of first-passage ideas to finance, in *First-Passage Phenomena and Their Applications* (World Scientific, 2014) Chap. 1, pp. 447–476.

[12] X. M. de Wit, A. van Kan, and A. Alexakis, *Bistability of the large-scale dynamics in quasi-two-dimensional turbulence,* Journal of Fluid Mechanics **939**, R2 (2022).

[13] N. F. Polizzi, M. J. Therien, and D. N. Beratan, *Mean first-passage times in biology,* Israel Journal of Chemistry **56**, 816 (2016).

[14] B. Meerson and S. Redner, *Mortality, redundancy, and diversity in stochastic search,* Phys. Rev. Lett. **114**, 198101 (2015).

[15] A. c. v. Godec and R. Metzler, *Universal proximity effect in target search kinetics in the few-encounter limit,* Phys. Rev. X **6**, 041037 (2016).

[16] I. Eliazar, T. Koren, and J. Klafter, *Searching circular dna strands,* Journal of Physics: Condensed Matter **19**, 065140 (2007).

[17] J. Szymanski and M. Weiss, *Elucidating the origin of anomalous diffusion in crowded fluids,* Phys. Rev. Lett. **103**, 038102 (2009).

[18] Y. Zhang and O. K. Dudko, *First-passage processes in the genome,* Annual Review of Biophysics **45**, 117 (2016), pMID: 27391924.

[19] C. Hyeon and D. Thirumalai, *Can energy landscape roughness of proteins and rna be measured by using mechanical unfolding experiments?* Proceedings of the National Academy of Sciences **100** (2003), 10.1073/pnas.1833310100.

[20] R. Nevo, V. Brumfeld, R. Kapon, P. Hinterdorfer, and Z. Reich, *Direct measurement of protein energy landscape roughness,* EMBO reports **6**, 482 (2005).

[21] K. Biswas, M. Shreshtha, A. Surendran, and A. Ghosh, *First-passage time statistics of stochastic transcription process for time-dependent reaction rates,* The European Physical Journal E **42**, 24 (2019).

[22] Y. Tu and G. Grinstein, *How white noise generates power-law switching in bacterial flagellar motors,* Phys. Rev. Lett. **94**, 208101 (2005).

[23] S. Dev and S. Chatterjee, *Optimal search in E. coli chemotaxis,* Phys. Rev. E **91**, 042714 (2015).

[24] O. Benichou, M. Coppey, M. Moreau, P.-H. Suet, and R. Voituriez, *Optimal search strategies for hidden targets,* Physical Review Letters **94**, 198101 (2005).

[25] T. Taillefumier and M. O. Magnasco, *A phase transition in the first passage of a Brownian process through a fluctuating boundary with implications for neural coding,* Proceedings of the National Academy of Sciences **110** (2013), 10.1073/pnas.1212479110.

[26] K. Pakdaman, S. Tanabe, and T. Shimokawa, *Coherence resonance and discharge time reliability in neurons and neuronal models,* Neural Networks **14**, 895 (2001).

[27] T. Spanio, J. Hidalgo, and M. A. Muñoz, *Impact of environmental colored noise in single-species population dynamics,* Phys. Rev. E **96**, 042301 (2017).

[28] J. P. Bouchaud, *Weak ergodicity breaking and aging in disordered systems,* J. Phys. I France **2** (1992), 10.1051/jp1:1992238.

[29] L. F. Cugliandolo and J. Kurchan, *Analytical solution of the off-equilibrium dynamics of a long-range spin-glass model,* Phys. Rev. Lett. **71**, 173 (1993).

[30] K. Binder and A. P. Young, *Spin glasses: Experimental facts, theoretical concepts, and open questions,* Reviews of Modern Physics **58**, 801 (1986).

[31] J. Jackle, *Models of the glass transition,* Reports on Progress in Physics **49**, 171 (1986).

[32] P. G. Debenedetti and F. H. Stillinger, *Supercooled liquids and the glass transition,* Nature **410**, 259 (2001).

[33] A. P. Young, *Spin Glasses and Random Fields*, Directions in condensed matter physics (World Scientific, 1997).

[34] A. X. Brown and B. de Bivort, *Ethology as a physical science,* Nature Physics **14**, 653 (2018).

[35] G. J. Berman, *Measuring behavior across scales,* BMC Biol. **16** (2018), 10.1186/s12915-018-0494-7.

[36] T. D. Pereira, J. W. Shaevitz, and M. Murthy, *Quantifying behavior to understand the brain,* Nature Neuroscience **23**, 1537 (2020).

[37] M. W. Mathis and A. Mathis, *Deep learning tools for the measurement of animal behavior in neuroscience,* Current Opinion in Neurobiology **60**, 1 (2020).

[38] E. Yemini, T. Jucikas, L. J. Grundy, A. E. Brown, and W. R. Schafer, *A database of Caenorhabditis elegans behavioral phenotypes,* Nat Methods **10** (2013), 10.1038/nmeth.2560.

[39] L. Hebert, T. Ahamed, A. C. Costa, L. O'Shaughnessy, and G. J. Stephens, *WormPose: Image synthesis and convolutional networks for pose estimation in C. elegans,*

PLoS Computational Biology **17**, e1008914 (2021).
[40] H. C. Berg, *E. coli in motion*, Biological and medical physics series (Springer, New York, 2004).
[41] G. J. Berman, D. M. Choi, W. Bialek, and J. W. Shaevitz, *Mapping the stereotyped behaviour of freely moving fruit flies.* J. Royal Soc. Interface **11**, 1 (2014).
[42] G. J. Stephens, B. Johnson-Kerner, W. Bialek, and W. S. Ryu, *Dimensionality and dynamics in the behavior of C. elegans.* PLoS Comput. Biol. **4**, e1000028 (2008).
[43] A. C. Costa, T. Ahamed, and G. J. Stephens, *Adaptive, locally linear models of complex dynamics,* Proceedings of the National Academy of Sciences of the United States of America **116** (2019), 10.1073/pnas.1813476116.
[44] T. Ahamed, A. C. Costa, and G. J. Stephens, *Capturing the continuous complexity of behaviour in Caenorhabditis elegans,* Nature Physics **17**, 275 (2021).
[45] A. B. Wiltschko, M. J. Johnson, G. Iurilli, R. E. Peterson, J. M. Katon, S. L. Pashkovski, V. E. Abraira, R. P. Adams, and S. R. Datta, *Mapping Sub-Second Structure in Mouse Behavior,* Neuron **88**, 1121 (2015).
[46] R. E. Johnson, S. Linderman, T. Panier, C. L. Wee, E. Song, K. J. Herrera, A. Miller, and F. Engert, *Probabilistic Models of Larval Zebrafish Behavior Reveal Structure on Many Scales,* Current Biology **30**, 70 (2020).
[47] V. Alba, G. J. Berman, W. Bialek, and J. W. Shaevitz, *Exploring a strongly non-markovian animal behavior,* (2020), arXiv:2012.15681 [q-bio.NC].
[48] A. C. Costa, T. Ahamed, D. Jordan, and G. Stephens, *Maximally predictive ensemble dynamics from data,* (2021), arXiv:2105.12811 [physics.bio-ph].
[49] J. T. Pierce-Shimomura, T. M. Morse, and S. R. Lockery, *The fundamental role of pirouettes in Caenorhabditis elegans chemotaxis.* J. Neurosci. **19**, 9557 (1999).
[50] N. Srivastava, D. a. Clark, and a. D. T. Samuel, *Temporal Analysis of Stochastic Turning Behavior of Swimming C. elegans,* Journal of Neurophysiology **102**, 1172 (2009).
[51] C. I. Bargmann, *Beyond the connectome: How neuromodulators shape neural circuits,* BioEssays **34**, 458 (2012).
[52] E. Marder, *Neuromodulation of Neuronal Circuits: Back to the Future,* Neuron **76**, 1 (2012).
[53] S. W. Flavell, N. Gogolla, M. Lovett-Barron, and M. Zelikowsky, *The emergence and influence of internal states,* Neuron **110**, 2545 (2022).
[54] J. M. Gray, J. J. Hill, and C. I. Bargmann, *A circuit for navigation in Caenorhabditis elegans,* Proceedings of the National Academy of Sciences **102** (2005), 10.1073/pnas.0409009101.
[55] H. Mori, *Transport, Collective Motion, and Brownian Motion,* Progress of Theoretical Physics **33** (1965).
[56] R. Zwanzig, *Nonlinear generalized Langevin equations,* Journal of Statistical Physics **9**, 215 (1973).
[57] D. S. Grebenkov, *First exit times of harmonically trapped particles: a didactic review,* Journal of Physics A: Mathematical and Theoretical **48**, 013001 (2014).
[58] A. J. F. Siegert, *On the first passage time probability problem,* Phys. Rev. **81**, 617 (1951).
[59] F. R. de Hoog, J. H. Knight, and A. N. Stokes, *An improved method for numerical inversion of laplace transforms,* SIAM J. Sci. Stat. Comput. **3**, 357–366 (1982).
[60] P. Mullowney and S. Iyengar, *Parameter estimation for a leaky integrate-and-fire neuronal model from ISI data,* Journal of Computational Neuroscience **24**, 179 (2008).
[61] P. Charbonneau, J. Kurchan, G. Parisi, P. Urbani, and F. Zamponi, *Fractal free energy landscapes in structural glasses,* Nature Communications **5**, 3725 (2014).
[62] R. Zwanzig, *Diffusion in a rough potential.* Proceedings of the National Academy of Sciences **85**, 2029 (1988).
[63] E. Korobkova, T. Emonet, J. M. G. Vilar, T. S. Shimizu, and P. Cluzel, *From molecular noise to behavioural variability in a single bacterium,* Nature **428**, 574 (2004).
[64] O. Miramontes, O. DeSouza, L. R. Paiva, A. Marins, and S. Orozco, *Lévy flights and self-similar exploratory behaviour of termite workers: Beyond model fitting,* PLOS ONE **9**, 1 (2014).
[65] K. Jung, H. Jang, J. D. Kralik, and J. Jeong, *Bursts and heavy tails in temporal and sequential dynamics of foraging decisions,* PLOS Computational Biology **10**, 1 (2014).
[66] N. E. Humphries, N. Queiroz, J. R. M. Dyer, N. G. Pade, M. K. Musyl, K. M. Schaefer, D. W. Fuller, J. M. Brunnschweiler, T. K. Doyle, J. D. R. Houghton, G. C. Hays, C. S. Jones, L. R. Noble, V. J. Wearmouth, E. J. Southall, and D. W. Sims, *Environmental context explains Lévy and Brownian movement patterns of marine predators,* Nature **465**, 1066 (2010).
[67] D. W. Sims, E. J. Southall, N. E. Humphries, G. C. Hays, C. J. A. Bradshaw, J. W. Pitchford, A. James, M. Z. Ahmed, A. S. Brierley, M. A. Hindell, D. Morritt, M. K. Musyl, D. Righton, E. L. C. Shepard, V. J. Wearmouth, R. P. Wilson, M. J. Witt, and J. D. Metcalfe, *Scaling laws of marine predator search behaviour,* Nature **451**, 1098 (2008).
[68] D. A. Raichlen, B. M. Wood, A. D. Gordon, A. Z. P. Mabulla, F. W. Marlowe, and H. Pontzer, *Evidence of lévy walk foraging patterns in human hunter–gatherers,* Proceedings of the National Academy of Sciences **111** (2014), 10.1073/pnas.1318616111.
[69] D. W. Sims, A. M. Reynolds, N. E. Humphries, E. J. Southall, V. J. Wearmouth, B. Metcalfe, and R. J. Twitchett, *Hierarchical random walks in trace fossils and the origin of optimal search behavior,* Proceedings of the National Academy of Sciences **111** (2014), 10.1073/pnas.1405966111.
[70] G. M. Viswanathan, S. V. Buldyrev, S. Havlin, M. G. da Luz, E. P. Raposo, and H. E. Stanley, *Optimizing the success of random searches.* Nature **401**, 911 (1999).
[71] M. E. Wosniack, M. C. Santos, E. P. Raposo, G. M. Viswanathan, and M. G. E. da Luz, *Robustness of optimal random searches in fragmented environments,* Phys. Rev. E **91**, 052119 (2015).
[72] M. E. Wosniack, M. C. Santos, E. P. Raposo, G. M. Viswanathan, and M. G. E. da Luz, *The evolutionary origins of lévy walk foraging,* PLOS Computational Biology **13**, 1 (2017).
[73] B. Guinard and A. Korman, *Intermittent inverse-square levy walks are optimal for finding targets of all sizes,* Science Advances **7**, eabe8211 (2021).
[74] A. Clementi, F. d'Amore, G. Giakkoupis, and E. Natale, in *Proceedings of the 2021 ACM Symposium on Principles of Distributed Computing*, PODC'21 (Association for Computing Machinery, New York, NY, USA, 2021) p. 81–91.
[75] D. W. Sims, N. E. Humphries, N. Hu, V. Medan, and J. Berni, *Optimal searching behaviour generated intrinsically by the central pattern generator for locomotion,* eLife **8**, e50316 (2019).

[76] M. S. Wheatland, P. A. Sturrock, and J. M. McTiernan, *The waiting-time distribution of solar flare hard x-ray bursts,* The Astrophysical Journal **509**, 448 (1998).

[77] G. Boffetta, V. Carbone, P. Giuliani, P. Veltri, and A. Vulpiani, *Power laws in solar flares: Self-organized criticality or turbulence?* Phys. Rev. Lett. **83**, 4662 (1999).

[78] J. M. Beggs and D. Plenz, *Neuronal avalanches in neocortical circuits,* Journal of Neuroscience **23**, 11167 (2003).

[79] M. Newman, *Power laws, pareto distributions and Zipf's law,* Contemporary Physics **46**, 323 (2005).

[80] T. Mora and W. Bialek, *Are Biological Systems Poised at Criticality?* Journal of Statistical Physics **144**, 268 (2011).

[81] J. Touboul and A. Destexhe, *Power-law statistics and universal scaling in the absence of criticality,* Phys. Rev. E **95**, 012413 (2017).

[82] V. Priesemann and O. Shriki, *Can a time varying external drive give rise to apparent criticality in neural systems?* PLOS Computational Biology **14**, 1 (2018).

[83] A. Proekt, J. R. Banavar, A. Maritan, and D. W. Pfaff, *Scale invariance in the dynamics of spontaneous behavior,* Proceedings of the National Academy of Sciences **109** (2012), 10.1073/pnas.1206894109.

[84] D. J. Schwab, I. Nemenman, and P. Mehta, *Zipf's law and criticality in multivariate data without fine-tuning,* Physical Review Letters **113**, 1 (2014).

[85] S. Fauve and F. Heslot, *Stochastic resonance in a bistable system,* Physics Letters A **97**, 5 (1983).

[86] E. Lanzara, R. N. Mantegna, B. Spagnolo, and R. Zangara, *Experimental study of a nonlinear system in the presence of noise: The stochastic resonance,* American Journal of Physics **65**, 341 (1997).

[87] M. Vergassola, V. E. Deneke, and S. D. Talia, *Mitotic waves in the early embryogenesis of ¡i¿drosophila¡/i¿: Bistability traded for speed,* Proceedings of the National Academy of Sciences **115** (2018), 10.1073/pnas.1714873115.

[88] D. G. Duffy, *On the numerical inversion of laplace transforms: comparison of three new methods on characteristic problems from applications,* ACM Transactions on Mathematical Software **19**, 333 (1993).